An Interactive Numerical Procedure for Rotor Aeroelastic Stability Analysis Using Elastic Lifting Surface

Kyung M. Yoo
Korea Institute of Aeronautical Technology, Korean Air
Seoul, Korea

Dewey H. Hodges and David A. Peters
Georgia Institute of Technology
Atlanta, Georgia

ABSTRACT

A thin lifting-surface code based on unsteady vortex lattice method coupled with a prescribed wake geometry has been developed and verified through a number of code validation procedures for applications to aeroelastic analysis of helicopter rotor blades. The present thin lifting-surface code has been subsequently coupled to a structural dynamic model of elastic hingeless rotor blades to analyze the stabilty behavior. This was done by using a moving block analysis and comparing the results predicted by 2-D theory. The effects of interblade unsteady wake dynamics beneath the rotor blades (including the far returning wake of both the reference blade and the preceding one) on aerodynamic loadings are essential. The result shows the possible reason of the overprediction of lead-lag damping by 2-D quasi-steady aerodynamics is due to lack of both the tip-relief effect and the unsteady wake dynamics effect among the blades.

Introduction

Aeroelasticity deals with the behavior of an elastic system in an airstream wherein there is a significant reciprocal interaction or feedback between deformation and flow. Moreover, rotorcraft aeroelasticity inevitably includes the hub loads which work through the various load paths into the rest of the aircraft. When the rotorcraft body motion such as the pitch, roll, longitudinal and lateral rigid body motions is added to the rotor problem, the stability phenomena that are often of most importance are ground resonance and air resonance. The blade flap motion and the rotor aerodynamics must be accurately included in an analysis of air resonance, since the flap stiffness and aerodynamics determine the frequency and damping of the body modes in flight (Ref. 1). The problem of aeromechanical instability of a helicopter on the ground and in hovering flight is a complex phenomenon involving both the rotor and body degrees of freedom in which the rotor lead-lag regressing mode which includes substantial body pitch and roll motion may become unstable (Ref. 2). The rotor progressing and regressing modes appear in the fixed system essentially as a wobbling of the disk, either forward or backward, with respect to the rotor direction. The sources of rotorcraft vibrations has been concluded that the vibrations are mainly due to higher harmonic rotor airloads, undesirable rotor-airframe interactions, and airframe resonances near excitation frequencies. The major two sources of rotor higher harmonic airloads are regarded as the one per revolution periodic variation in velocity tangential to the lifting surface due to forward flight speed, and the rapid variations in velocity normal to the lifting surface due to vortex wake shed from both the reference blade and preceeding blades (Ref. 3). The strength and location of shed vortices become time-dependent due to even any small amount of rotorcraft attitude change. These vortices which results from the variation of circulation along the blade span and trails in helical form behind the blades locally induce unsteady airloadings associated with rotor transient responses since the rotor blade undergoes severe aeroelastic deformations and rapid changes in flow conditions.

Observations of the experimental research (Ref. 4) revealed that higher harmonic airloads due to complex induced-flow effects could be attributed to three major factors: 1) three-dimensionl effects in the plane of the rotor, such as the vorticity which results from the variation of circulation along the blade span and trails in helical form behind the blades, 2) the effect of vorticity which has been shed and blown below the rotor disc and which shoud be passed over by succeeding blades in succeeding revolutions, and 3) the effect of vorticity shed by previous blades and in previous revolutions. So, it can be safely stated that the accurate modeling of unsteady aerodynamic loads required for aeroelastic analyses including interblade wake dynamics continues to be one of the major challenges for rotary wing aeroelasticians.

A wide array of mathematical models starting from simple one and computationally intensive ones has been developed and applied to simulate the complex phenomena of rotor unsteady flowfield (Ref. 5). There

Presented as Paper ICAS-92-6.6.3 at the 18th ICAS Conference, Beijing, China, Sept. 20-25, 1992

has been done much research efforts by lifting surface method using vortex filament theory. Most of the efforts has been concentrated to the prediction of rigid-blade rotor performance and free wake geometry for tip vortex relocation. The direct consequence of the lift on a lifting surface in three-dimensional or unsteady flow is a wake of trailing and shed vorticity. This wake vorticity, in turn, induces a velocity at the lifting surface that has a major influence on the loading. The calculation of the wake-induced velocity is therefore an important part of rotary wing aerodynamic analyses. Considering both accuracy and efficiency, the calculation of the wake-induced velocity is often accomplished for the helicopter rotor by modeling the wake as a series of discrete elements. For each vortex element in the wake, the induced velocity is evaluated by analytical expressions; and, then, the total induced velocity is obtained by summing the contributions from all elements. Calculations of the rotor nonuniform inflow are thus based on the induced velocities due to discrete elements of the wake. However, only a limited number of application using lifting surface (Ref. 6) or lifting body aerodynamics (Ref. 7) was reported for the computation of rotor unsteady airloads undergoing harmonic or arbitrary perturbed motions and for the prediction of rotorcraft aeroelastic stability.

The aim of the present work is investigation of the role of unsteady wake dynamics and three-dimensional tip-relief effects for elastic rotor system eigenvalues. For investigating the interblade vortex-phasing effect on rotorcraft dynamics, a diffrent unsteady three-dimensional model that can capture not only the near wake but also the far wake (including both trailing vortices and shed vortices) which is eventually passing below the elastically deformable reference blade is still required. In addition, there exist inherently different dynamic modes in rotors such as collective, teetering, reactionless (differential), cyclic progressing, and cyclic regressing mode. Thus, to develop an unsteady model suitable for rotorcraft dynamics, a prerequisite is the accurate computation of the wake induced velocity along with the resulting airloads and blade motion for various kinds of helicopter rotor system.

In the present formulation, rotor blades are regarded as thin lifting surfaces. These thin lifting surfaces and the wake region are discretized by a number of vortex filaments piecewise constant strength. The unsteady strengths of all vortex elements are determined by a time-marching solution procedure. The paths of these unsteady vortex elements are prescribed to make the solution procedure linear. The panel density and the number of discretized wake elements are limited for computational efficiency. For the prediction of steady loading, a lifting surface can be divided into hundreds of vortex panels; but, for the prediction of unsteady loadings, the number of vortex panels and unsteady wake elements are severely limited due to computational time and memory requirements. To investigate the role of unsteady wake for rotor aeroelasticity, the wake elements trailed and shed from both the reference and the preceding blade undergoing different motions are taken into consideration up to a finite number of revolutions.

Aeroelastic Analysis of Elastic Rotor by Lifting Surface Theory in Hover

For hovering rotors, the 3N nonlinear, nonhomogeneous, constant-coefficient ordinary differential equations are linearized for small perturbation motions about the equilibrium operating conditions. The coefficient of these

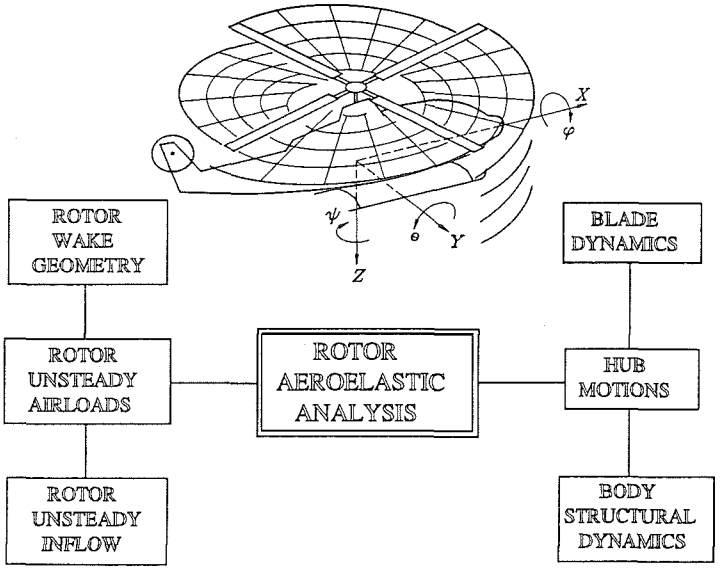

Fig. 1 Interactive Analysis Module of Rotor Aeroelastic Analysis

linearized perturbation equations define the unsteady blade motion near the equilibrium operation condition. The coefficients of these linearized perturbation equations define the unsteady blade flapping motion near the equilibrium operation condition. In the case for which quasi-steady theory aerodynamics is used to calculate the dynamic residual vector, the aeroelastic analysis can be performed by computing the steady-state hover response and by obtaining the matrices describing the sensitivity of the residual force vector F to perturbations about the equilibrium state. Then, the mass, damping/gyroscopic, and stiffness matrices, which depend upon the rotor angular speed, the blade properties, and the assumed modes in the analysis, are obtained for eigen analysis which yields structural dynamic behavior of the rotor sytem. The local stability of the steady-state response is then described by the equation

$$[M]\{\ddot{z}\}+[C]\{\dot{z}\}+[K]\{z\}=\{0\} \tag{1}$$

This linear second order system is converted to first order by defining the state vector

$$\{\Delta Z\}=\begin{Bmatrix}\Delta z\\ \Delta\dot{z}\end{Bmatrix}$$

so that the homogeneous equation becomes

$$\{\Delta\dot{Z}\}=\begin{bmatrix}0 & I\\ -[M]^{-1}[K] & -[M]^{-1}[C]\end{bmatrix}\{\Delta Z\}=[P]\{\Delta Z\} \tag{2}$$

Then, the system stability can be determined from the eigenvalues of the system modal matrix [P] stated above (Ref. 8).

Unlike quasi-steady aerodynamics theory, lifting surface aerodynamics does not have explicit aerodynamic damping and aerodynamic stiffness terms since all the velocity terms enter the right-hand-side as boundary conditions which specify the normal velocity of the elastic thin lifting surface. Therefore, we have

$$[M]\{\ddot{z}\}+[C]\{\dot{z}\}+[K]\{z\}=\{f\} \tag{3}$$

where

$$\{f\}=\begin{Bmatrix}-\frac{\gamma}{6a}\cos^2\beta_{pc}\int_0^1\bar{x}^2C_D(\bar{x},t)\Psi_i d\bar{x}\ (+\text{viscous})\\ +\frac{\gamma}{6a}\cos^2\beta_{pc}\int_0^1\bar{x}^2C_L(\bar{x},t)\Psi_i d\bar{x}\\ +\frac{\gamma\bar{c}^2}{6a}\cos^2\beta_{pc}\int_0^1\bar{x}^2C_M(\bar{x},t)\Theta_i d\bar{x}\end{Bmatrix}$$

where {f} represents the generalized force due to aerodynamic forces. Thus, the damping [C] and stiffness [K] matrices lack aerodynamic terms, which makes an eigenvalue analysis impossible. Furthermore, the dynamic residual of each time step becomes very different from that of quasi-steady aerodynamic theory since the magnitude and phase differences in lift create aerodynamic damping in an implicit way. The system stability can be obtained,

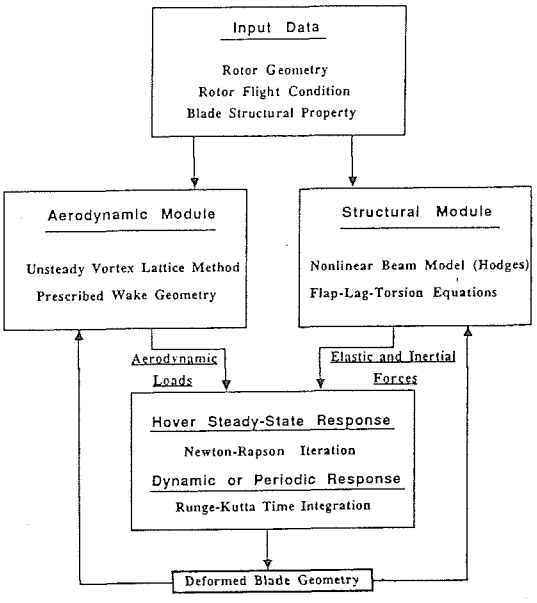

Fig. 2 Block Diagram of the Present Aeroelastic Analysis

however, through a numerical perturbation of Δz about its equilibrium state. Then, by tracing all the time histories of motions, one can thus obtain input data appropriate for the Fourier analyzer (Ref. 9) which yields damping and frequency values of blade motions. The perturbation equations are homogeneous, constant-coefficient ordinary differential equations of the form

$$[M]\{\Delta\ddot{z}\}+[C]\{\Delta\dot{z}\}+[K]\{\Delta z\}=\{\Delta f\} \tag{4}$$

where Δz contains the perturbed quantities of blade motion; and Δf represents the small perturbed quantities of aerodynamic forces which are calculated in real time base from the input of perturbed Δz. When the blade is moving in air, the aerodynamic forces become nonlinear functions of both the elastic blade deformations and the relative velocity due to the blade motion at each instant of time. The effect of past force history is accounted for by consideration of the time-dependent wake vorticies which are generated due to the time and spanwise variation of the blade bound vorticies.

Once the equilibrium deflections are determined, the coefficient matrices, [M], [C], and [K] can be found, and the generalized force can be calculated from the known equilibrium blade deflections and the blade properties. To start the numerical perturbation procedure, initial perturbation of displacement and velocity are required. The magnitude of numerical perturbation of these deflections is a few percent of equilibrium deflection respectively. To investigate the rotor damping, the blade perturbation is given; and then the blade is set free to move under the interaction of internal, inertial, and external aerodynamic forces. At each time step, from the known values of state vector and force term, the blade

geometry and the total velocity impinging on the blade local surface can be determined by a numerical integration routine such as the 5th or 6th order Runge-Kutta-Verner method. Since the different velocity impinging on the elastic blade, the AIC should be computed at each time step to include the effect of derformation and to update its normal boundary condition due to the perturbation. This would be rather expensive; and it is fortunate that, when the perturbation is only few percent, the numerical result of using the AIC (aerodynamic influence coefficient) computed at the equilibrium state shows only a small difference with that of the AIC updated at each time step as long as the normal boundary condition is updated at each time step.

Thus, an interactive numerical procedure is formulated for tracking the physical variations in time domain both of the in the flow field and elastic rotor blades to analyze the aeroelastic stability.

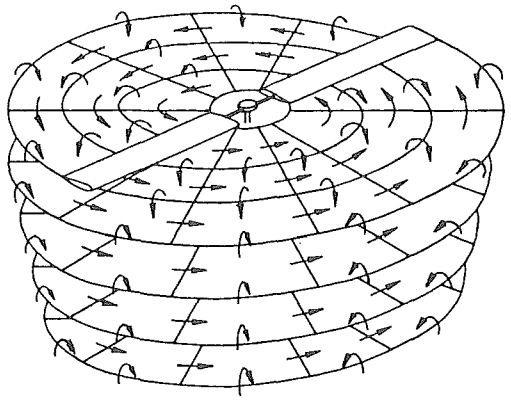

Fig. 3 Schematics of the Unsteady Wake

This theorem postulates that the circulation Γ around a closed circuit which moves with the fluid is constant. This integral derivation actually implies that any transient change in the circulation of the blade is compensated by the shedding of vorticity opposite sign. The induced velocity is the sum of all trailing and shed wake vortex filaments. The strength of unsteady trailing and shed wake segments is obtained by spanwise difference and timewise difference of the chordwise sum of bound vorticity of each panel, respectively. For example, at a time equal to t - Δt, the strength of one segment of trailing and shed vortex filament becomes as follows (Ref. 10).

$$\Gamma_{T,n}(r,t-\Delta t) = \sum_{mn}^{M}\Gamma^{B}\left(r_{j+1},t-\Delta t\right) - \sum_{mn}^{M}\Gamma^{B}\left(r_{j},t-\Delta t\right) \qquad (6)$$

$$\Gamma_{S,n}(r,t-\Delta t) = \sum_{mn}^{M}\Gamma^{B}\left(r_{j},t\right) - \sum_{mn}^{M}\Gamma^{B}\left(r_{j},t-\Delta t\right) \qquad (7)$$

The control point is at mid-span and three-quarter chord

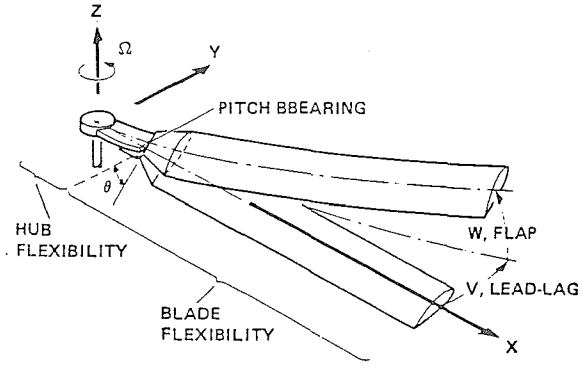

Fig. 4 Schematics of Hingeless Rotor Blade

Formulation of Interactive Numerical Procedure

As the rotor blade moves, it sets the air in motion. As a result, vorticity is created in the boundary layers of the upper and lower surfaces and vortices are formed along the sharp edges. These vortices are shed and convected away from the blade surface and constitute the wake. To calculate the instantaneous strength of the streamwise vortex sheet, shed at the trailing edge, Kelvin's theorem is applied. This theorem postulates that the circulation around a closed circuit which moves with the fluid is constant. This integral derivation actually implies that any transient change in the circulation of the blade is compensated by the shedding of vorticity opposite sign.

$$\left(\frac{d\Gamma}{dt}\right)_{blade} + \left(\frac{d\Gamma}{dt}\right)_{wake} = 0 \qquad (5)$$

of each rectangular element of the bound vortex surface, which satisfies the Kutta condition implicitly. The boundary condition of no flow penetration is satisfied at this control point of each element. The instantaneous induced velocity at any point on the rotor blade surface will be a sum of all the velocities induced by the vortex elements as shown in equation (8).

$$\left(\frac{\partial\Phi}{\partial z}\right)_{surface} = -\frac{\Gamma}{4\pi}\oint_{surface+wake}\frac{\vec{r}\times d\vec{l}}{|\vec{r}^{3}|} \qquad (8)$$

After the kinematic analysis of the deformed rotor blade, the perpendicular velocity components ($\vec{v}_S\cdot\vec{n}$) impinging on the deformed lifting surface at each collocation point becomes the right hand side of equation (9) which includes the normal component of the perturbed freestream and one

due to flapping, pitching and lead-lag motion of the elastic rotor blade as well as one due to rigid blade motion. To satisfy no flow penetration across the collocation point of the lifting surface, the total sum of the induced veocity by the bound and wake filaments and total kinematic normal velocity should vanish at each collocation point in hovering flight as follows.

$$\frac{\Gamma}{4\pi}\iint_{\text{surface+wake}}\frac{\vec{r}\times d\vec{l}}{|\vec{r}^3|} = \vec{v}_s\cdot\vec{n} \qquad (9)$$

$$=-\Omega x(\theta+\phi)+\dot{w}+\Omega v(\beta_{pc}+w')-(\theta+\phi)\dot{v}-\xi(\dot{\theta}+\dot{\phi})\cos\beta_{pc}$$

where ξ is the relative chordwise distance between the elastic axis and collocation point of each panel. Previous rotor blade applications with two-dimensional quasi-steady theory do not have the last term $\xi(\dot{\theta}+\dot{\phi})\cos\beta_{pc}$ which represents an unsteady normal velocity due to pitching rotation and chordwise offset. After discretizing the lifting surface into panel elements, the previous equation can be expressed in a simplified marix form

$$[B]\{\Gamma\} = \left\{\vec{v}_s\cdot\vec{n}\right\} - \{w\}_{total} \qquad (10)$$

where [B] represents an AIC matrix due to the unit strength bound vortex Γ of each panel and {W} is the total induced velocity contributed by all trailing and shed wake filaments. For a two-bladed rotor undergoing arbitrary transient motions, as mentioned before, there are two different modtions depending upon flight conditions such as collective, teetering (cyclic differential), respectively. Thus, a formulation that can treat the interblade phase difference is required. Equation (10) can be expressed as follows for a two-bladed rotor (See reference 6 for multi-bladed rotor cases).

$$\begin{aligned}
&\left[B^{ij}_{mn}\right]^R\Gamma^B_{mn}(r,t) = \left\{\vec{v}_S\cdot\vec{n}\right\}^R \\
&-\left[T^{ij}_{kn}\right]^R\left[\sum_{k=1}^{Rev}\Gamma_{T,n}(r,t-k\Delta t)\otimes\left\{\Psi_q\right\}^R\right] \\
&-\left[S^{ij}_{kn}\right]^R\left[\sum_{k=1}^{Rev}\Gamma_{S,n}(r,t-k\Delta t)\otimes\left\{\Psi_q\right\}^R\right] \\
&-\left[T^{ij}_{kn}\right]^{P1}\left[\sum_{k=1}^{Rev}\Gamma_{T,n}(r,t-k\Delta t)\otimes\left\{\Psi_q\right\}^{P1}\right] \\
&-\left[S^{ij}_{kn}\right]^{P1}\left[\sum_{k=1}^{Rev}\Gamma_{S,n}(r,t-k\Delta t)\otimes\left\{\Psi_q\right\}^{P1}\right]
\end{aligned} \qquad (11)$$

where (i,m) represents the chordwise, and j represents spanwise panel number of blade surface and (k,n) represents the timewise, spanwise number of wake segments due to a finite number of revolutions. [T], [S] represents AIC matrices due to the individual unit strength trailing and shed wake filaments of each blade. Also, R and P1 represent the reference blade and preceding blade, respectively. The differential strength of wake vortex filaments multiplied by AIC gives some finite out-of-phase normal velocity component on each collocation point of the lifting surface panels.

To simulate the interblade phase difference, a phase control matrix is introduced as $\{\Psi_q\}$ which actually makes the release of each vortices' memory to be delayed dependent on each blade phase. For a teetering mode, for example, the phase of reference blade and preceding blade (P1) has 180 deg phase difference which implies those blade wake vortices have opposite sign of strength compared to reference one. After an initial transient revolution, the interblade phase difference effects are clearly demonstrated in the flowfield.

In forward flight, trailing and shed wake AIC must be computed as function of radial and azimuthal to the wake geometry, whereas in hover it can be computed once in rigid blade. When a non time-varying (rigid) blade is considered, bound vortex AIC can be computed once; but, when a time-dependent (elastic) blade is considered, every bound vortex AIC should be computed at each time step. However, when perturbed motions are small in the rotor blade in hover with respect to equilibrium positions, the wake AIC do not have to be iterated at each time step because wake geometry changes only a small amount due to the small fluctuations of the blade motions. The time-dependent boundary condition of no flow penetration must be updated at each time step.

The solution of the algebraic matrix equation gives the bound vortex strength of each element at each time step which determines the local pressure jump on the blade surface as expressed in equation (12). The detailed local chordwise pressure jump can be obtained if enough chordwise panel number are used. The amount of computational time is related to the total number of blade panels, number of wake revolutions, and number of time steps.

$$\Delta p_j(t) = \frac{2\rho}{S_j}U(t)\int_0^c\frac{\partial\Phi}{\partial x}dx\Delta y_j \qquad (12)$$

where i indicates the spanwise section and c, S represent its sectional chord, and area, respectively. This can be rewritten in terms of the panel chordwise unsteady bound circulation as follows.

$$\Delta F_j(t) = \Delta p_j(t)\cdot S_j = 2\rho U(t)\int_0^c\frac{\partial\Phi}{\partial x}dx\Delta y_j \qquad (13)$$

The resulting sectional unsteady aerodynamic loadings about the aerodynamic center are obtained by integrating each normal force along the blade surface.

Results and Discussions

To investigate the effect of wake alignment on the vibratory airloadings beneath the rotor blades, the cyclic differential plunging hub motions having integer-multiple of frequency ratio ($N = \omega/\Omega$) were added to a two-bladed

rigid rotor in the collective mode. The collecive pitch angle is set to 8° which determines the wake helix departure angle. The lifting surface is discretized as one chordwise and eight spanwise bound vortex filaments, and each blade has each 4 wake layers below the rotor disc. Figure 5 shows the time history of the perturbed generalized lift from the results of two-dimensional quasi-steady aerodynamics and the present method. In the case of N=1 hub motion, the two blades oscillate in phase and generate in-phase vortices. Thus, in this case, the unsteady vortices shed from the preceding blade arrive at the reference blade after one-half revolution make the induced inflow out-of-phase which means cancelling effect of wake-induced flow (small lift loss). The perturbed airloading is mainly influenced by near wake vortices.

In the case of N=2 hub motion, the trend is reversed from that for frequency ratio 1. The in-phase vortices shed from the preceding blade pass below the reference blade in phase. This in-phase inflow causes the unsteady lift fluctuation to be smaller than that of N=1 case, as shown

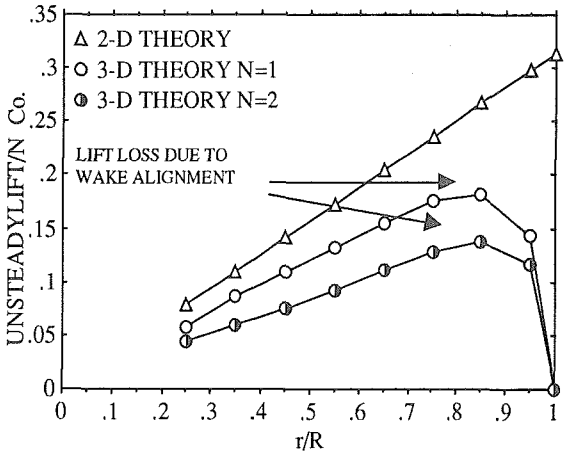

Fig. 7 Spanwise Lift Distribution at Peak

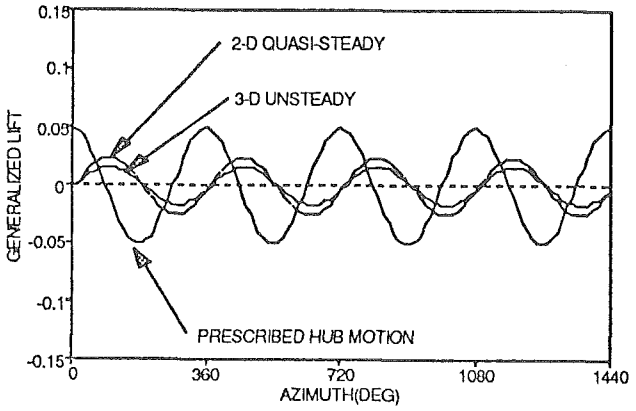

Fig. 5 Time Histories of the Perturbed Lift (N=1)

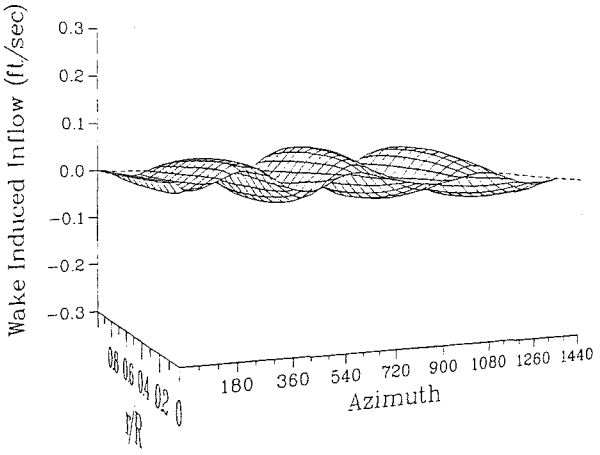

Fig. 8 3-D Plot of Wake-Induced Inflow by Reference Blade

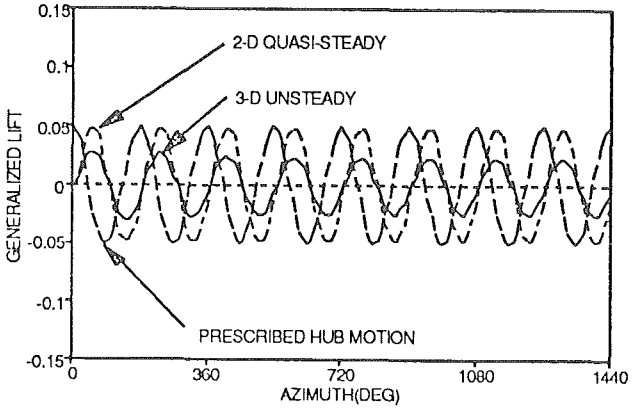

Fig. 6 Time Histories of the Perturbed Lift (N=2)

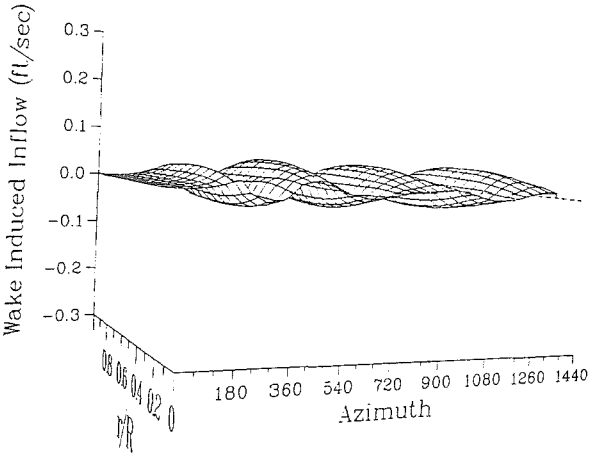

Fig. 9 3-D Plot of Wake-Induced Inflow by Preceding Blade

in Figure 6 because the vortices shed from the reference and preceding blade have same sign of strength when they pass below the refence blade. Figure 7 shows the spanwise lift distribution of these two cases. At the outboard section, clear lift loss due to the strong tip vortex of near wake is observed for both two frequency ratios. But for the N=2 case, more lift loss is observed by the in-phase shed vortices. Thus, the rigid hingeless two-bladed rotor experiences an abrupt lift loss at even integer exicitation frequency in the collective mode. However, the quasi-steady theory is modified version of two-dimensional airfoil theory could not observe the vortex-phasing phenomena beneath the rotor disc regardless of rotor blade motions, which leads to predict larger magnitudes of thrust.

For two-bladed rotors in hovering flight, there are two kinds of dynamic motion - the collective mode and the teetering (cyclic differential) mode. In the teetering mode, one blade is moving in an upstroke, while the other one is moving in a downstroke; in the collective mode both blades are subjected to the same motion. Thus, the unsteady vortex strength of each wake grid is dependent on the mode. In a teetering mode, matrices of vortex strength of the wake of the preceding blade have equal magnitude and opposite sign of those of the reference blade. Figure 8-9 shows two 3-D representations of induced inflow velocities due to the shed wake of both the reference blade and preceding blade. As shown in the figure, the induced inflow produced by this kind of unsteady wake is dependent on the individual mode of the two-bladed rotor subsection From Figure 9, it is noticed that after half revolution the wake-induced inflow by the preceding blade has some magnitude since the vortices generated by the preceding blade takes half revolution to reach the reference blade.

Figures 10-11 show the time histories of flapping response and flapping motion-induced generalized lift in the teetering mode at a collective pitch $\theta = 2°$. Because two-dimensional quasi-steady theory produces larger flapping-induced lift due to the lack of the tip-relief effect and the unsteady wake effect, the response obtained by quasi-steady theory decaies earlier. The larger velocity (90° phase lag with displacement) implicitly couples with larger aerodynamic damping forces which are dependent on velocities of blade motions. This also proves that the two-dimensional quasi-steady theory is not suitable for rotor craft aeroelastic anaysis. Figure 12 shows the phase plane of flapping velocity and displacement during the residual transient period at low collective pitch angle. As expected, the locus predicted by the present theory shows slow convergence due to lift loss than that of quasi-steady one (Ref. 11).

As discussed earlier, the time histories of numerically perturbed lead-lag, flap and torsion equations yield damping and frequency values through the use of the moving block analysis. Figures 13-15 show the time histories of lead-lag, flap and torsional perturbed motion at 8 deg collective pitch. Once the equilibrium deflections are determined, the coefficient matrices, [M], [C], and [K] can

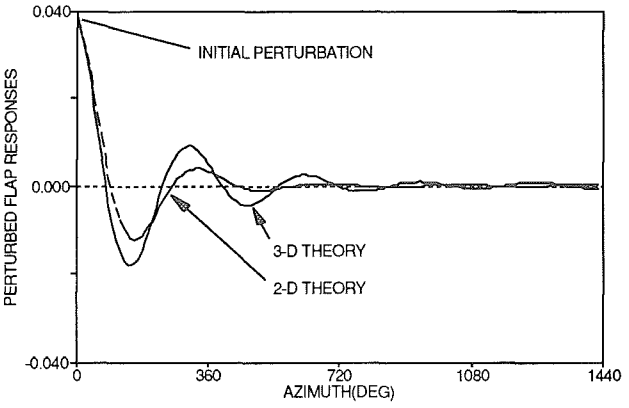

Fig. 10 Time Histories of Transient Flap Responses (Collective Pitch 2 Deg)

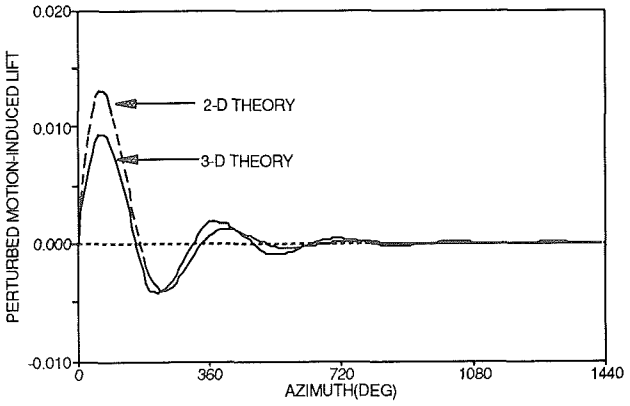

Fig. 11 Time Histories of Flap Motion-Induced Lift (Collective Pitch 2 Deg)

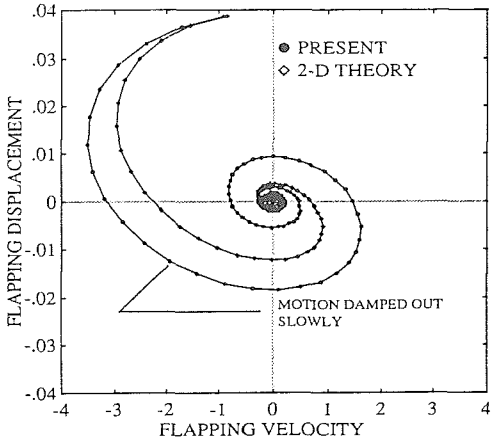

Fig. 12 Locus of Convergence

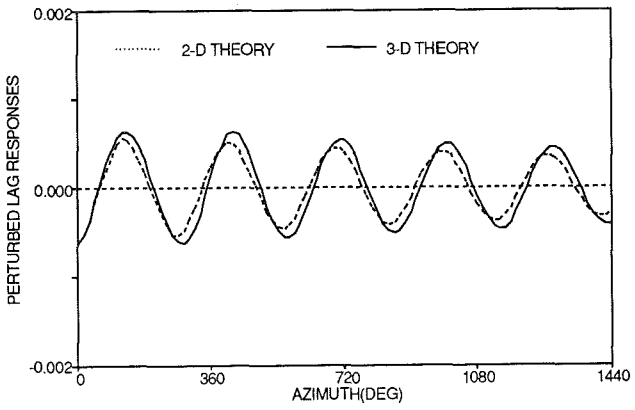

Fig. 13 Time History of the Perturbed Lead-Lag Motion

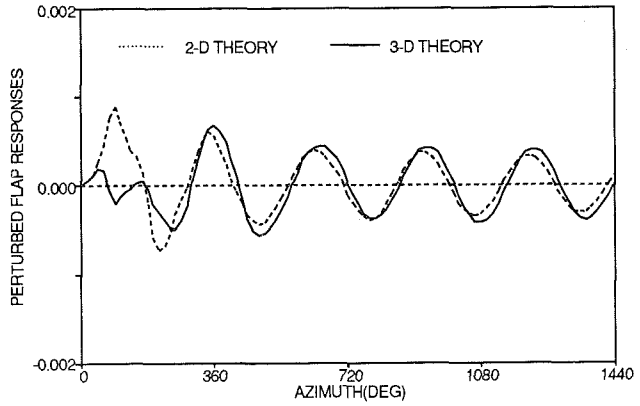

Fig. 14 Time History of the Perturbed Flap Motion

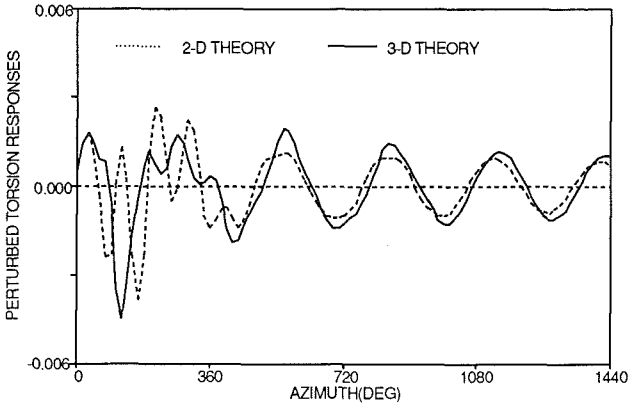

Fig. 15 Time History of the Perturbed Torsional Motion

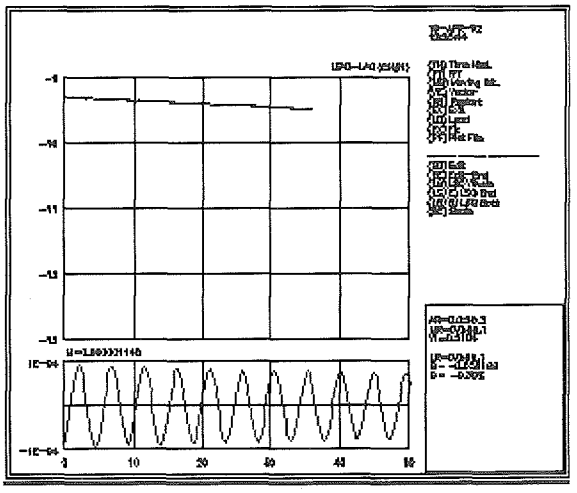

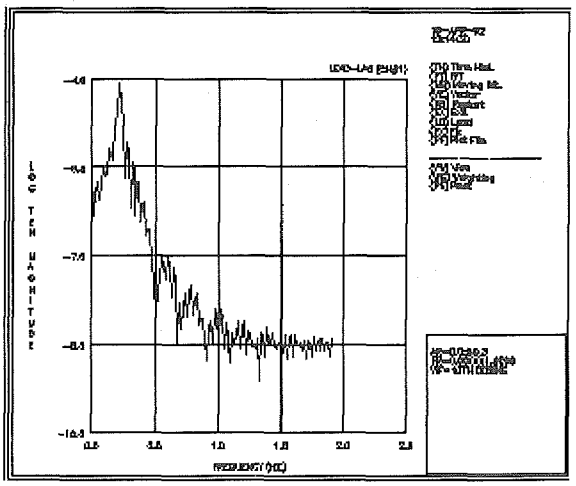

Fig. 16 Frequency Response by Moving Block Analysis

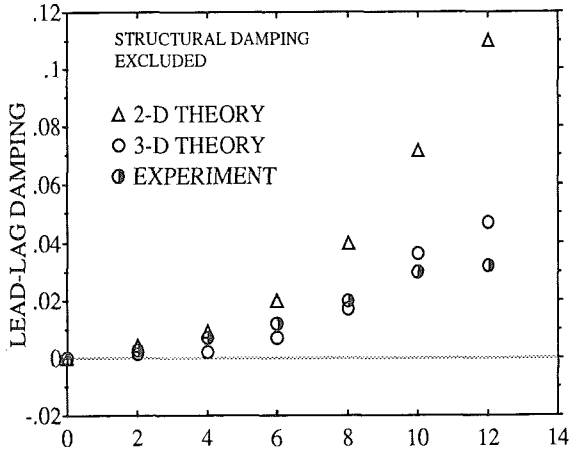

Fig. 17 Comparison of Lead-Lag Dampings

be found, and the generalized forces and moment can be calculated from the known equilibrium blade deflections and the blade properties.

To start the numerical perturbation procedure, initial perturbations of displacements and velocities are required. The magnitude of numerical perturbation of these deflections is a few percent of equilibrium deflection respectively. A small value is used so that nonlinearities do not enter. To investigate the lead-lag damping, only the lead-lag perturbation is given; and then the blade is set free to move under the interaction of internal, inertial, and external aerodynamic forces. The initial values of velocity and force are assumed as zero at time $t = 0$, since at the maximum lead-lag deflection, it can be assumed that the lead-lag velocity and the residual drag are at a minimum.

At each time step, from the known values of state vector and force term, the blade geometry and the total velocity impinging on the blade local surface can be determined by a numerical integration routine. Once the time histories of lead-lag, flap and torsional deflection are obtained, the modal damping and frequency can be determined using the moving block analysis as in Figure 16 which shows the frequency response of particular lead-lag mode is plotted. When the rotor blade has highly coupled motions, it is recommended that a particular mode of interest for each of the lead-lag, flap or torsion deflections is perturbed initially and then the subsequent motion is analyzed to obtain the modal damping and frequency for that particular motion and mode. The rotor blade used for the present computation is a simplified rotor that was suggested by Sharp (Ref. 12) for an analytical study. Figure 17 show the comparison of the lead-lag damping. The damping from the present method shows a lower value than ones from the damping from two-dimensional aerodynamics. Experimental measurement of lead-lag damping was performed in teetering mode excitation, which means more lift loss due to wake alignment beneath the reference blade in odd number of mode frequency. The present interactive numerical modeling could capture the interblade wake alignment whereas the two-dimensional theory took constant wake-induced inflow regardless of blade motions. This difference of the lead-lag damping is expected to be larger if the flapping and torsional frequencies are to be interger multiples.

Conclusions

The present thin lifting-surface code has been subsequently coupled to a structural dynamic model of elastic hingeless rotor blades to analyze the stabilty behavior. This was done by using a moving block analysis and comparing the results predicted by 2-D theory. The unsteady wake effects on rotor aeroelastic stability are essential. The result shows the reason of the overprediction of lead-lag damping by 2-D quasi-steady aerodynamics is due to lack of tip-relief effect, the unsteady wake dynamics effect including returning and far wake of all blades. Coclusively, without inclusion of the interblade rotor wake effect, the predction of rotor stability would lead to inaccurate results.

References

[1]Johnson, W., "Recent Developments in the Dynamics of Advanced Rotor Systems," NASA TM-86669, March 1985

[2]Bousman, W. G., " An Experimental Investigation of the Effects of Aeroelastic Couplings on Aeromecanical Stability of a Hingeless Rotor Helicopter," *Journal of American Helicopter Society,* Vol. 26, No. 1, January 1981

[3]Yen, J. G., Yuce, M., Chao, C-F., and Schillings, J., "Validation of Rotor Vibratory Airload and Application to Helicopter Response," *Journal of American Helicopter Society,* Vol. 35, No. 4, October 1990

[4]Theodorsen, T. and Regier, A. A., "Effect of the Lift Coefficient on Propeller Flutter," NACA ACR L5F30, July, 1954.

[5]Peters, D. A., "Modeling of Unsteady Aerodynamics for Rotary-Wing Aeroelasticity," *Proceedings of the 6th International Conference on the Mathematical Modelling,* St. Louis, Missouri, August 4-7, 1987

[6]Yoo, K. M., "Prediction of Rotor Unsteady Airloads Using Vortex Filament Theory," *Proceedings of the 10th AIAA Applied Aerodynamics Conference,* AIAA-92-2610, Palo Alto, CA., June 22-24, 1992

[7]Kwon, O. J., Hodges, D. H., and Sankar, L. N., "Stability of Hingeless Rotors in Hover Using Three-Dimensional Unsteady Aerodynamics," *Journal of American Helicopter Society,* Vol. 36, No. 2, April 1991

[8]Hodges, D. H. and Ormiston, R. A., "Stability of Elastic Bending and Torsion of Uniform Cantilever Rotor Blades in Hover with Variable Structural Coupling," NASA TN D-8192, May 1976

[9]Bousman, W. G. and Winkler, D. J., "Application of the Moving--Block Analysis," *Proceedings of 22nd AIAA/ ASME/ASCE/AHS Structures, Structural Dynamics and Materials Conference* , April 1981, pp. 775-763.

[10]Yoo, K. M., "A Time-Marching Numerical Procedure for Rotor Vibratory Airloadings," DGLR/AAAF/AIAA/ RAeS *International Forum on Aeroelasticity and Structural Dynamics,* Paper 91-067, Eurogress Center, Aachen, Germany, June 3-6, 1991

[11]Yoo, K. M., "Unsteady Wake Effect on Rotor Vibratory Airloadings," *Proceedings of the AHS/RAeS International Technical Specialists' Meeting on Rotorcraft Acoustics and Rotor Fluid Dynamcis,* Philadelphia, PA., October 15-17, 1991.

[12] Sharpe, D. L. "An Experimental Investigation of the Flap-Lag-Torsion Aeroelastic Stability of a Small-Scale Hingeless Helicopter Rotor in Hover", NASA Technical Paper 2546, 1986